Robot-Assisted Surface Finish of STAVAX Mold Steel with Constant Force Control Using Lab-Made Polishing Tools

Fang-Jung Shiou*, Chang-Mou Wu**, Wei-Yu Shih*** and Bo-Yu Chen***

Keywords:

six-axis industrial robot, polishing tool, constant force polishing, PID control, Taguchi method, STAVAX mold steel.

ABSTRACT

The automated precision surface finishing processes are the demanding technologies to be developed, to improve some drawbacks of manual polishing. The objective of this study is to develop robot assisted constant force polishing of STAVAX mold steel using lab-made polishing tools mounted on a new polishing end effector. A new polishing end effector embedded with a force sensor has been designed and fabricated, so constant force polishing was possible on a 6-axis industrial robot. The Taguchi method was applied to determine the optimal polishing parameters of the new polishing tools for the STAVAX mold steel. For flat plane polishing using a cylindrical polishing tool with a diameter of 40 mm, the appropriate parameters were the particle size of 0.3 μm, a rotation speed of 5,600 rev/min, a feed rate of 0.1 mm/min, and a polishing force of 6 N. The PID controller has been adopted in this work for constant

Paper Received July, 2025. Revised August, 2025. Accepted August, 2025. Author for Correspondence: Fang-Jung Shiou.

* Professor, Department of Mechanical Engineering, National Taiwan University of Science and Technology, Taipei, Taiwan 106335, ROC.

email: shiou@mail.ntust.edu.tw

** Professor, Department of Material Science and Engineering, National Taiwan University of Science and Technology, Taipei, Taiwan 106335, ROC. email: cmwu@mail.ntust.edu.tw

*** Graduate Student, Department of Mechanical Engineering, National Taiwan University of Science and Technology, Taipei, Taiwan 106335, ROC.

email: m10903236@mail.ntust.edu.tw

**** Graduate Student, Department of Mechanical Engineering, National Taiwan University of Science and Technology, Taipei, Taiwan 106335, ROC.

email: m10703232@mail.ntust.edu.tw

force polishing. The control gains of Kp, Ki, and Kd of the PID controller were investigated by polishing experiments for different polishing tools. The optimal polishing parameters were applied to both the flat and freeform surfaces of a test carrier. Based on the experimental results, the surface roughness of the plane area was improved from Ra 0.36 μm to Ra 0.02 μm after sequential burnishing and polishing. For a freeform surface area, the surface roughness of the burnished test carrier was reduced from Ra 0.18 μm to Ra 0.04 μm on average after ball polishing.

INTRODUCTION

Most of the surfaces of mould inserts or mold cavities used for forming and shaping processes for the final stage finishing process in the industry are polished manually by an experienced technician. Some drawbacks, such as unstable finishing results, no standardized process strategies, shortage of skilled experts, and adverse health effects, etc., are encountered problems for manual polishing. As a result, the automated precision surface finishing processes are the demanding technologies to be developed. The machine tools used for automated mechanical freeform surface finishing processes mainly include the robots and the 5-axis machining centre, depending on the size of the mold. Robot assisted polishing is suitable for the medium-sized or large-sized workpiece considering the difficulty of clamping and movement of the workpiece on a machine tool.

As an alternative or supplement to the conventional manual polishing process in the manufacturing of dies or moulds, robot-assisted polishing technology was investigated in (Wang et al., 2019). The recent advanced techniques of the robot-assisted polishing were reviewed in (Ke et al. 2023), such as bonnet polishing, small tool polishing, fluid jet polishing, magnetorheological polishing, rigid comfortable tool polishing, and water-jet polishing etc. The Bonnet polishing technology was developed by the ZEEKO company and the University of London

for the ultraprecision polishing of large optical components and freeform surfaces (Wu et al. 2022). A robot assisted bonnet polishing control model was proposed to polish large-diameter axisymmetric aspherical optical components in (Huang et al. 2022). A new center-inlet computer-controlled robotic polishing system is developed for large-diameter aspheric optics on a 5-DOF hybrid robot (Lin et al. 2019). A robotic polishing system with an end-effector equipped with a magnetorheological fluid damper was proposed to achieve consistent force output while reducing spindle vibration in (Xu and Hu 2023). A sequential robot fluid jet polishing and robot pad polishing on a steel mould surface improvement for polymer optic production was proposed in (Almeida et al. 2019). The robotic polishing of NAK80 mold steel using an adaptive hydraulic polishing equipped robotic platform with 3M abrasive discs of progressively refined grit sizes was systematically investigated in (Shi et al. 2025). Regarding the development of polishing tools, a new sol-gel flexible polishing pads have been developed to polish complex marble surfaces on a robot in (Huang et al. 2025). The new lab-made rubber polishing balls including the aluminum oxide abrasive were developed to polish STAVAX mold steel on a 5-axis CNC machining center in (Shiou et al. 2023). With regard to path planning on a robot, a method for the optimal path planning for robotic polishing of sheet metal parts is purposed in (Liu et al. 2022), to achieve the entire surface without over or under polishing force. A tool trajectory planning method for robot assisted polishing of complex surfaces was developed in (Xiao et al. 2022), to achieve the desired material removal depths on the workpiece surface. Concerning the constant force control for robotic polishing, a novel cooperative force-position control method was proposed in (Li et al. 2023), to implement the normal contact force control. The constant force control polishing method on an industrial robot equipped with six-dimensional force/torque sensors is proposed to maintain stable force achieved by a position-based impedance control algorithm in (Chang et al. 2022). A pneumatic polishing force loading control system for variable polishing force on a hybrid robot was adjusted by the moving average filter PID control method in (Shi et al. 2020).

For the pre-machining processes of the workpiece before polishing, A sequential ball grinding, ball burnishing and ball polishing processes on a machining center for the surface finishing of a hardened stainless tool steel was reported in (Shiou and Hsu 2008). During the robotic grinding and polishing processes, a variable impedance control approach is proposed in (Li et al. 2025), to improve the accuracy and stability of force tracking. To determine the optimal combination of polishing parameters for a mold steel on a 6-axis industrial robot, such as polishing pressure, rotational speed of polishing tool,

feed rate, etc., the Taguchi method was adopted in (Li et al. 2024). There is no polishing pads or polishing balls, made of nitrile butadiene rubber (NBR) mixing with the abrasive of aluminium oxide, have been studied to be integrated with a robot to perform the surface finish after a workpiece has been burnished.

The objective of this work is to develop a robot assisted constant force polishing using the NBR-based lab-made polishing tools clamped on a new polishing end effector, to improve the surface roughness of a burnished STAVAX mold steel. A new polishing end effector including a force sensor and an electrical grinder designed for a 6-axis industrial robot, integration of the polishing end effector with the robot, the property of the STAVAX stainless mold steel, the development of the lab-made rubber-based polishing pads and balls embedded with the abrasive of aluminium oxide, configuration of the Taguchi matrix experiment, and PID control for the constant force polishing are introduced in the section of experimental work and methodology. The experimental results on the suitable polishing parameters for different polishing tools, appropriate PID control parameters for constant force polishing, application of the constant force polishing to the surface finishing of a test carrier with a plane surface and a freeform surface, volumetric wear of the polishing tools and discussion are reported in the section of results and discussion.

EXPERIMENTAL WORK AND METHODOLOGY

Design of a New Polishing End Effector Embedded with a Force Sensor

In this study, a polishing end-effector suitable for integration with a robotic arm was developed. The tool features both force overload protection and force detection capabilities to achieve constant-force polishing. An exploded view of the polishing endeffector and its components is shown in Figure 1. Component 2 is the upper mounting plate, used to secure the tool to the flange of the robotic arm; component 3 is a six-axis force/torque sensor, type Robotiq FT-300; component 5 is a mold spring; and component 6 is an outer casing with a U-shaped sliding groove that defines the tool's stroke. The electric grinder (component 10) is mounted on the designed fixture (component 9). Different lab-made polishing tools were clamped on the spindle of the electric grinder. The motion mechanism involves the stroke of component 6 moving upward to the limit of the U-shaped groove, during which the spring compresses to provide an overload protection effect for the force sensor. By adjusting the spring constant (K value) and limiting the stroke range, the sensing force can be maintained at a fixed value, thus preventing sudden excessive loads that may damage the force sensor. The maximum polishing force was set at 10 N in this work. Given the spring constant of 2.78 kg/mm, the appropriate stroke length of the U-shaped groove was calculated based on Hook's Law to be 0.3 mm, and this value was adopted for the stroke limit in the design.

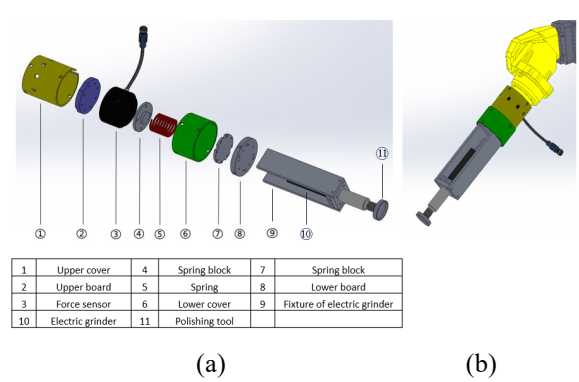


Fig. 1. (a) Exploded view and components of the polishing end effector embedded with a force sensor (b) assembly view.

To evaluate the deformation and stress distribution of the polishing end-effector under load, a finite element analysis was conducted using ANSYS software. In the simulation a polishing force of 30 N - three times the maximum design load - was applied in the simulation. The results, shown in Figure 2, revealed a maximum deformation of approximately 0.002 mm and a maximum stress of approximately 322.09 MPa, which is below the yield strength (~ 400 MPa) of the medium-carbon steel S45C used for the adjusting chamber of the electric grinder.

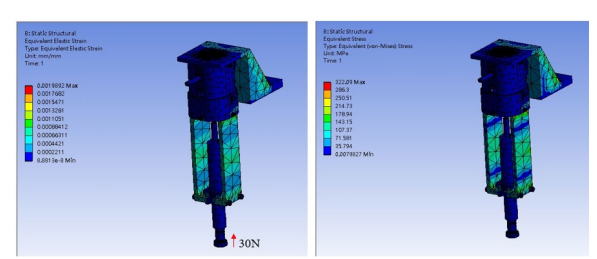


Fig. 2. Simulation of the end effector with a load of 30 N (a) Induced deformation (b) induced stress.

Integration of the Polishing Tool with the CNC Turning Center

The assembled polishing end effector was integrated with the 6-axis robot, type FANUC M-10iA, equipped with the FANUC R-30i controller, as shown in Figure 3. The robot positioning accuracy was about 0.10 mm and the maximum payload was 10 kg. A PID force control system programmed with the C# language was developed and connected to the FANUC R-30i controller, to make constant force polishing possible. The NC codes needed for fine milling, ball burnishing and polishing paths were simulated and generated by the Unigraphics NX 10.0 CAD/CAM software. After simulation of the machining path, these generated NC codes can then be transmitted to the

CNC machining center controller and robot via RS232 serial interface. The surface roughness of the workpiece after the fine milling, burnishing, and polishing processes was measured using the Hommelwerke T8000 roughness and contour tester, made by JENOPTIC (Jena, Germany).

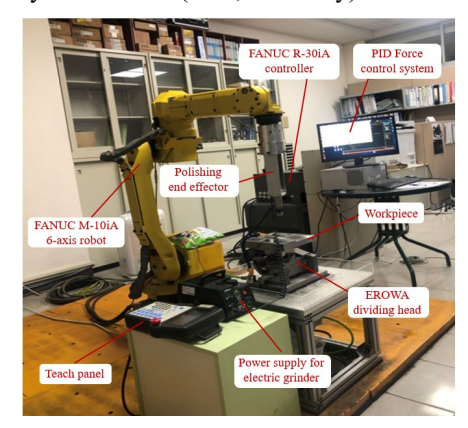


Fig. 3. System integration of the fabricated polishing end effector and PID control system with the 6-axis robot.

Material and Specimen Preparation

The STAVAX stainless mold steel used in this study includes corrosion and wear resistance with excellent properties in polishing, machinability, and hardening stability (STAVAX ESR 2025). Table 1 shows the chemical composition of the used STAVAX stainless steel. The hardness of this material is about HRC20 after tempering.

Table 1. Chemical composition of STAVAX stainless steel (%) (STAVAX ESR 2025).

Composition	С	Si	Mn	Cr	V
%	0.38	0.9	0.5	13.6	0.3

A medium-sized test carrier with a plane surface and a freeform surface feature was designed, as shown in Figure 4. In this study, the sequential fine milling, burnishing, and polishing processes of STAVAX mold steel were adopted. The fine milling and burnishing processes of the workpiece were implemented in a CNC machining center.

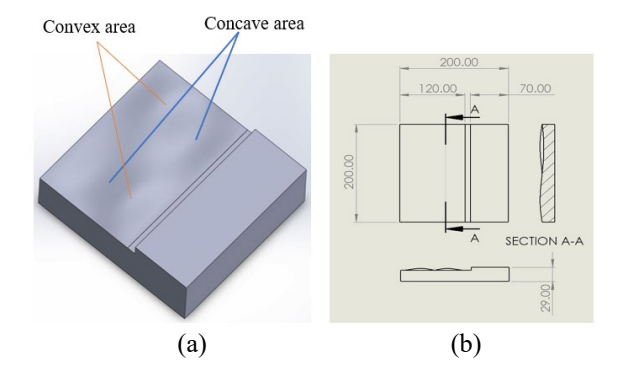


Fig. 4. Design of the test carrier (a) 3D CAD model (b) dimension of the test carrier.

Development of the Lab-made Polishing Tools Embedded with the Abrasive of Aluminum Oxide

In this study a new abrasive-embedded polishing tool has been developed, considering environmental protection, so that a slurry circulation system will not be used. The abrasive of aluminum oxide (Al₂O₃) is suitable for polishing the STAVAX stainless mold steel, according to the results of the previous study (Shiou et al. 2023). Consequently, a new polishing tool embedded with aluminum oxide abrasive has been developed taking nitrile butadiene rubber (NBR), Styrene butadiene rubber (SBR) and Butadiene Rubber (BR) as a matrix, mixing with aluminum oxide abrasive with different sizes (0.05 to 3 um) and concentration and additives, as indicated in Table 2. Concerning the good physical, mechanical, and chemical properties, such as abrasion resistance, adhesion to metal, compression set, tear resistance, vibration dampening, solvent resistance, etc., the NBR has been selected as the main matrix material. Five types of NBR-based blanks were made after the NBR. abrasives of different sizes, and some additives were homogenously mixed by a blending machine.

Table 2. Composition of the polishing rubbers and additives

udditi v e B				
Rubber matrix (%)	Nitrile butadiene rubber (NBR)	50.0		
	Styrene butadiene rubber (SBR)	14.3		
	Butadiene rubber (BR)	7.1		
Additives (%)	Silicon Oxide (Hi-Sil 233)	14.3		
	Aluminum oxide	14.3		

Two types of molds made of Al-6061T6 with HRB 54 hardness have been designed and fabricated to fabricate the polishing tools, as shown in Figure 5. Different types of polishing ball with a diameter of 20 mm (PB20) and polishing pads with a diameter of 20 mm (PD20) and 40 mm (PD), respectively, have been manufactured by thermal forming processes. Figure 6 illustrates the fabricated polishing tools mounted on the polishing end effector to execute the polishing work.

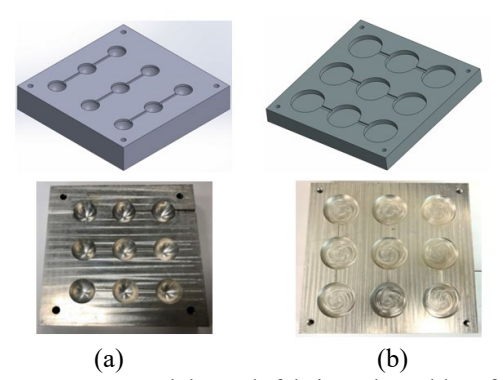


Fig. 5. CAD models and fabricated molds of the

polishing tools (a) PD20 polishing balls (b) PD40 polishing pad

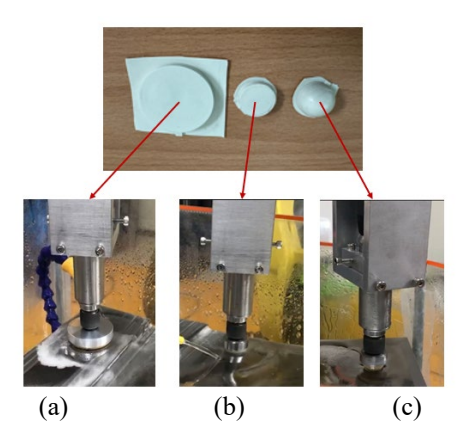


Fig. 6. Fabricated lab-made polishing tools mounted on the polishing end effector (a) polishing pad PD40 (b) polishing pad PD20 (c) polishing ball PB20.

To carry out constant force polishing, the polishing force with respect to the depth of penetration for the fabricated polishing tools were calibrated, so that the displacement of a polishing tool can be determined based on the regression line of calibration. The polishing force was measured with the Robotiq FT-300 sensor with a resolution of 0.1 N. Figure 7 presents the calibration result of the polishing ball with a diameter of 20 mm. The linear regression line equation was y = 9.89x + 0.33. The R-squared value of 0.9985 was nearly perfect fit for the polishing ball PB20. The calibration result of the polishing pad with a diameter of 40 mm is demonstrated in Figure 8. The linear regression line equation was y =73.25x - 1.60. The R-squared value of 0.957 was very good fit for the polishing ball PD40. Figure 9 presents the calibration result of the polishing pad with a diameter of 20 mm. The linear regression line equation was y = 43.59x - 0.33. The R-squared value of 0.9747 was very good fit for the polishing ball PD20.

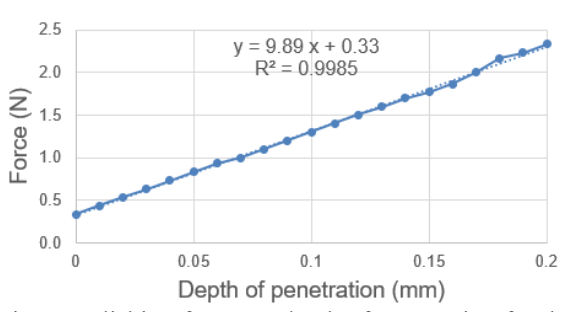


Fig. 7. Polishing force vs. depth of penetration for the polishing ball PB20.

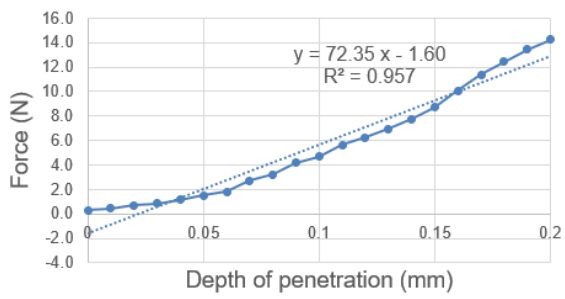


Fig. 8. Polishing force vs. depth of penetration for the polishing pad PD40.

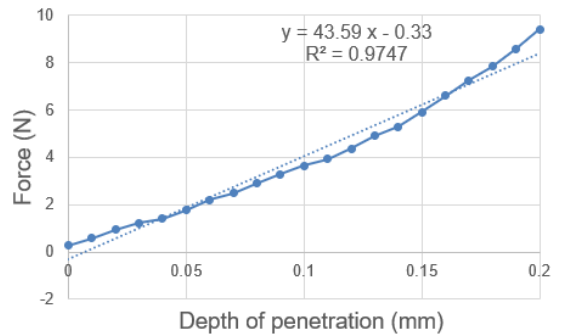


Fig. 9. Polishing force vs. depth of penetration for the polishing pad PD20.

Configuration of the Taguchi Matrix Experiment

The suitable polishing parameters of the newly lab-made polishing tools for both the polishing ball with diameter of 20 mm (PB20) and the polishing pad with diameter of 40 mm (PD40) were determined by executing the Taguchi matrix experiments. The control factors and levels of the polishing ball with a diameter of 20 mm have been configured with an orthogonal table L18 (2¹ X 3⁴) with one factor for two levels and four factors for three levels. The configuration table is shown in Table 3. In total of five main factors, namely the abrasive size, spindle speed, feed rate, polishing force, and stepover. The abrasive materials used were aluminum oxide (Al₂O₃) with diameters of 1.0 µm and 0.05 µm, respectively. The spindle speeds were 7,000, 8,000, and 9,000, individually. Three numerical values of the rest of the four factors were determined based on the pre-study results. The L18 orthogonal matrix was selected to conduct matrix experiments for four 3level factors and one 2-level factor.

The control factors and levels of the polishing pad with a diameter of 40 mm to polish a plane have been configured with an orthogonal table L9 (3⁴) with four factors for three levels. The configuration table is shown in Table 4. In total, four main factors are taken into account, namely, the abrasive size, the spindle speed, the feed rate and the polishing force. The stepover of 4.0 mm was set as 10 % of the diameter. Three numerical values of the four factors were determined based on the preliminary test results. The L9 orthogonal array was selected to conduct the matrix experiments for four 3-level factors.

Table 3 Configuration of the factors and levels for the polishing ball with diameter of 20 mm

Et	Level			
Factor	1	2	3	
A. Abrasive size (μm)	1	0.05		
B. Spindle speed (rev/min)	7,000	8,000	9,000	
C. Feed rate (mm/min)	45	60	75	
D. Force (N)	1.0	1.5	2.0	
E. Stepover (mm)	0.01	0.02	0.03	

Table 4 Configuration of the factors and levels for the cylindrical polishing pad with diameter of 40 mm

- J				
Г	Level			
Factor	1	2	3	
A. Abrasive size (μm)	0.3	0.5	3	
B. Spindle speed (rev/min)	5,600	6,600	7,600	
C. Feed rate (mm/min)	0.1	0.6	1	
D. Force (N)	5.0	6.0	7.0	

The S/N ratio for the smaller-the better type problem, η , is defined by the following equation (Phadke 2015),

$$\eta = -10 \log_{10} \left[\frac{1}{n} \sum_{i=1}^{n} y_i^2 \right] \tag{1}$$

 y_i : observations of the quality characteristic under different noise conditions

n: number of experiments

The optimization strategy for the smaller-thebetter problem is to maximize η defined by equation (1). Levels that maximize η will be selected for the factors that have a significant effect on η . The optimal conditions for polishing tools can then be determined.

PID Control for the Constant Force Polishing

During robotic polishing processes, several factors can prevent the polishing tool from maintaining a consistent contact force with the work surface. These issues can arise from robotic positioning errors, tool wear, coordinate system transformation inaccuracies, or discrepancies between the actual workpiece and its CAD model. To address this problem, a constant-force control method can be implemented to achieve constant-force polishing.

In this study, the widely adopted PID (Proportional-Integral-Derivative) force control method is employed, with its formulas shown in Equations (2) and (3) (Diaz-Rodriguez et al. 2019). The control block diagram is illustrated in Figure 10. When the polishing tool moves to the initial position, the program activates the controller. Upon reaching the second position, the system begins to receive average sensed force data. If the polishing force deviation falls within the preset range of ± 0.2 N, no correction is applied. However, if the force deviation exceeds this

range, the PID controller calculates the compensation displacement u(t) based on the force error e(t) and sends the correction value to the robot controller for position adjustment, thus achieving force-controlled polishing. To evaluate the force error e(t), in addition to calculating the difference between the desired force and the current force measured by the force sensor, the gravitational force of the polishing end effector was also considered by measuring the force at different positions along the polishing path without the polishing force. In this study, the PID controller operates at a sampling frequency of 10 Hz, with compensation calculations performed at intervals of 0.1 mm. For simplification, the time interval Δt in Equation (3) is set to 1 second. The test specimens used for polishing include both planar and freeform surface features. Different types of rubber polishing tools and appropriate polishing strategies are selected according to the features of the surface.

$$u(t) = Kp \ e(t) + Ki \ \int_0^t e(t) \ dt + Kd \ \frac{d \ e(t)}{dt} \quad (2)$$

$$u(t) \approx Kp \ e(t) + Ki \sum_{i=0}^{t} e(i) \ \Delta t_i + Kd \ \frac{[e(t) - e(t-1)]}{\Delta t}$$
(3)

Where,

e(t): force errorKp: proportional gainKi: integral gainKd: derivative gain

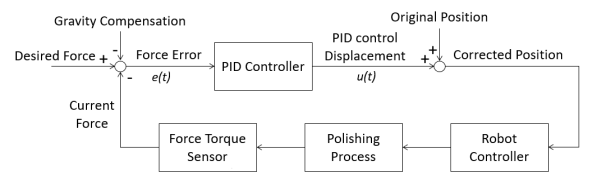


Fig. 10. Block diagram of PID control for constant polishing force.

The compensation displacement is calculated along the normal surface direction of each polishing point, as described in Equation (4). In the control program, the correction value computed by the PID controller is multiplied by the three components of the unit normal vector (*Nx, Ny, Nz*). The resulting values are added to the X, Y, and Z coordinates of the subsequent point, and the updated position is then transmitted to the robot controller to complete the toolpath correction. A portion of the code used to calculate the compensation displacement is shown in Figure 11.

$$CorrP_{nosition} = CurrP_{nosition} + (D \times nVec_{nosition})$$
 (4)

 $CorrP_{position}$: corrected position $CurrP_{position}$: current position

D: Displacement calculated by PID control, u(t) $nVec_{vosition}$: unit normal vector at current position

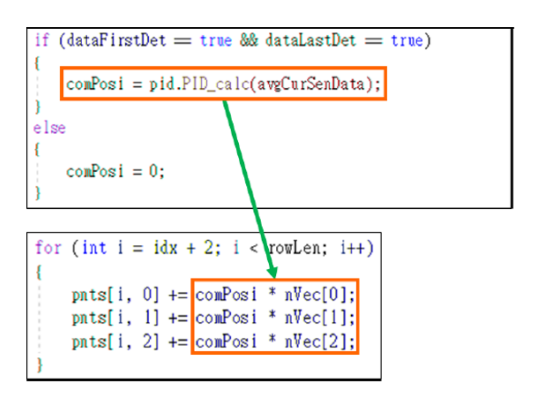


Fig. 11. Partial code snippet for compensation displacement calculation in PID control.

RESULTS AND DISCUSSION

Suitable Combination of Polishing Parameters for Different Polishing Tools

The objective in the robot-assisted polishing process is to minimize the surface roughness value of the polished specimens by determining the optimal level of each factor. Given that $-\log$ is a monotonically decreasing function, it means that maximizing the S/N ratio is required. As a result, we can determine the optimal level for each factor as the level that has the maximum value of η . For the polishing ball with the diameter of 20 mm, the combination of the optimal level for each factor was A2B1C3D1E1, as shown in Figure 12. The combination of the optimal lab-made ball polishing parameters was the abrasive size of 0.05 μ m, the spindle speed of 7,000 rpm, feed rate of 75 mm/min, polishing force of 1 N, listed in Table 5.

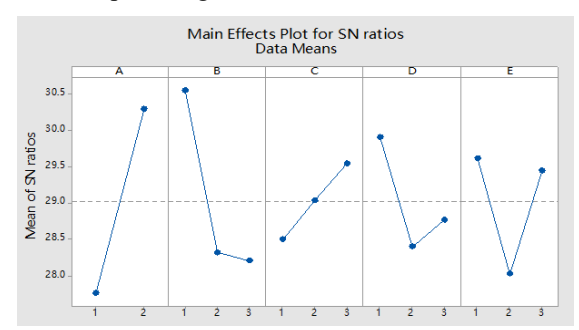


Fig. 12. Signal-to-noise (S/N) ratio plot from Taguchi analysis for the 20 mm polishing ball (optimal factor levels A2B1C3D1E1).

Table 5. Combination of the optimal lab-made PB20 ball polishing parameters.

Factor	Level
A. Abrasive size (μm)	0.05
B. Spindle speed (rev/min)	7,000
C. Feed rate (mm/min)	75
D. Polishing force (N)	1.0
E. Stepover (mm)	0.01

For the polishing pad with a diameter of 40 mm, the combination of the optimal level for each factor

was A1B1C1D2, as shown in Figure 13. The combination of the optimal lab-made ball polishing parameters was the abrasive size of $0.3 \mu m$, the spindle speed of 5,600 rpm, feed rate of 0.1 mm/min, polishing force of 6.0 N, listed in Table 6.0 N

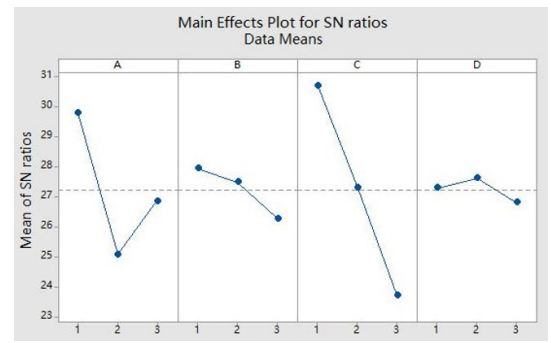


Fig. 13. Signal-to-noise (S/N) ratio plot from Taguchi analysis for the 40 mm polishing pad (optimal factor levels A1B1C1D2).

Table 6. Combination of the suitable lab-made polishing pad PD40 parameters.

Factor	Level
A. Abrasive size (μm)	0.3
B. Spindle speed (rev/min)	5600
C. Feed rate (mm/min)	0.1
D. Polishing force (N)	6

For the polishing pad with a diameter of 20 mm, the combination of the appropriate parameters is summarized in Table 7, based on the experimental results in (Shih 2023).

Table 7. Combination of the optimal lab-made polishing pad PD20 parameters

Factor	Level
A. Abrasive size (μm)	1
B. Spindle speed (rev/min)	6600
C. Feed rate (mm/min)	0.6
D. Polishing force (N)	5
E. Stepover (mm)	2.0

Suitable PID Control Gains for Constant Force Polishing

The polishing force determined for the individual polishing tool, based on the Taguchi experiment result, was used to find the corresponding gains of the PID controller. For the polishing pad with a diameter of 40 mm (PD40), the constant polishing force was set to 6.0 N, obtained in Table 6. The proportional gain Kp, the integral gain Ki, and the derivative gain Kd were experimentally investigated. Figure 14 presents the detected force signal using the PI control (Kp=0.025 and Ki=0.015) for the polishing tool PD40. The polishing force was controlled within $6.0 \text{ N} \pm 0.2 \text{ N}$ after 100 sec. By adding a small amount of derivative gain (Kd=0.0001) to the PID controller, the polishing force became uncontrollable with

increasing time, as shown in Figure 15. As a result, the PI control was used for the PD40 polishing pad.

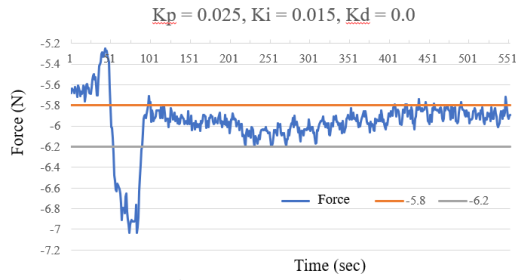


Fig. 14. Optimal PI control parameters for the polishing pad PD40.

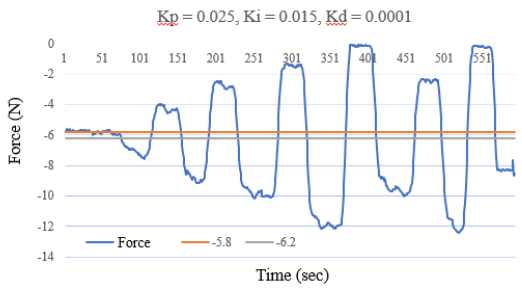


Fig. 15. Force response with PID control for polishing pad PD40 showing instability over time.

Similar to the polishing pad with a diameter of 20 mm (PD20), the constant polishing force was set at 5.0 N, obtained in Table 7. The proportional gain Kp and the integral gain Ki were experimentally investigated without using derivative control. Figure 16 shows the observed force signal using the PI control (Kp=0.02 and Ki=0.005) for the PD20 polishing tool. The polishing force was controlled stably at 5.0 N with some overshoots after 150 s. Consequently, the PI control was used for the PD20 polishing pad.

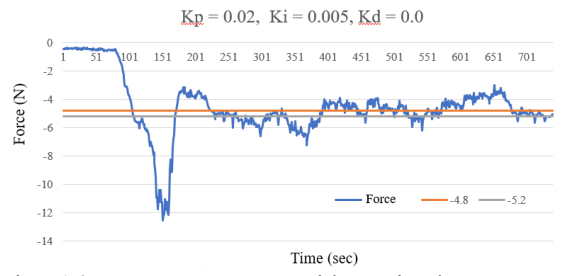


Fig. 16. Force response with optimal PI control (Kp=0.02, Ki=0.005) for polishing pad PD20.

The constant polishing force was set at 1.0 N obtained in Table 5, for the polishing ball with diameter of 20 mm (PB20). The proportional gain Kp was experimentally investigated without using the integral control and derivative control. Figure 17 shows the observed force signal using the P control (Kp=0.1) for the polishing toolPB20. The polishing force was controlled stably at 1.0 N with some overshoots after 50 s. Subsequently, the P control was used for the polishing pad PB20.

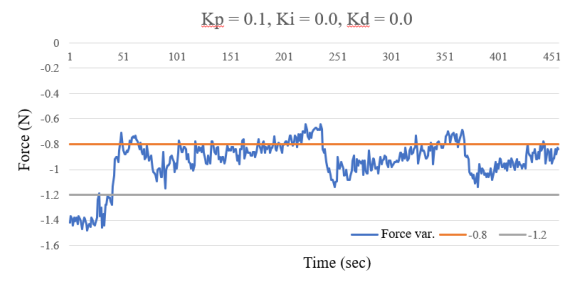


Fig. 17. Force response with proportional (P) control (Kp=0.1) for polishing ball PB20.

Table 8 summarized the corresponding gains of the PID controller with regard to different polishing tools that are to be applied to the surface finish of the test carrier with a plane and a freeform surface feature.

Table 8 Optimal PID control gains for different polishing tools

Polishing tools	Kp	Ki	Kd
Polishing pad dia. 40 mm	0.025	0.015	0
Polishing pad dia. 20 mm	0.02	0.005	0
Polishing ball dia. 20 mm	0.1	0	0

Application of the Constant Force Polishing to the Surface Finishing of a Test Carrier

The new developed polishing end effector clamping the lab-made polishing tools was applied to perform the precision surface finishing of the STAVAX mold steel test carrier (Figure 4), using the proposed constant force PID control. The premachining of the test carrier using sequential fine milling and ball burnishing was executed on a 5-axis machining. On the plane surface area, the fine milled surface roughness was improved from Ra 0.36 μm to 0.08 μm on average after ball burnishing. On the convex area, after ball burnishing the fine milled surface roughness was improved from Ra 0.89 μm to 0.18 μm on average. On the concave area, after ball burnishing the fine milled surface roughness was improved from Ra 0.85 μm to 0.12 μm on average.

The test carrier polishing path simulations using different lab-made polishing tools in different areas were carried out using Unigraphics NX 10.0 CAD/CAM software, as shown in Figure 18, to avoid a collision between the polishing tool and the workpiece. After finishing the polishing path simulations of the test carrier, the position coordinates of the NC codes were converted to the six rotational angles θ_1 to θ_6 , using the inverse kinetics calculation (Chen 2021).

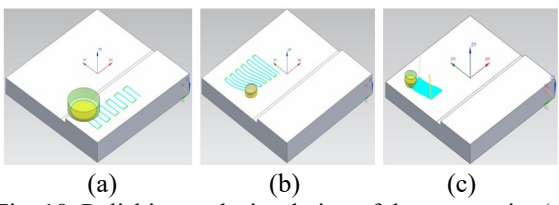


Fig. 18. Polishing path simulation of the test carrier (a)

Polishing pad PD40 on the plane area (b) Polishing pad PD20 on the convex and concave area (c) Polishing ball PB20 on the concave area.

The suitable polishing parameters (Table 6) of the polishing PD40 and the PI control (Kp=0.025 and Ki=0.015) were applied to polish the plane area. The burnished surface roughness improved from Ra 0.08 μm to 0.02 μm on average after polishing. Figure 19 presents the measured surface roughness of Ra 0.02 μm . The improvement in surface roughness of the polished plane surface was about 75%.

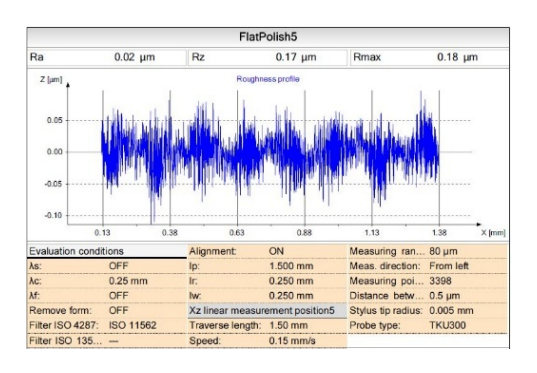


Fig. 19. Measured surface roughness of the polished plane area of test carrier using D40 polishing pad.

The suitable polishing parameters (Table 7) of the PD20 polishing pad and the PI control (Kp=0.02 and Ki=0.005) were applied to polish the freeform surface, including the convex and concave areas. The burnished surface roughness in the convex area improved from Ra 0.18 μ m to 0.04 μ m on average after polishing. Figure 20 presents the measured surface roughness of Ra 0.04 μ m. The improvement in surface roughness of the polished plane surface was approximately 78%.

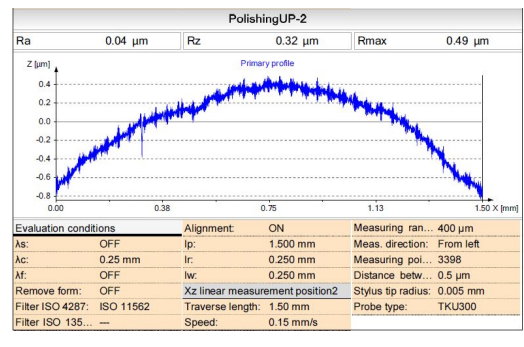


Fig. 20. Measured surface roughness of the polished convex area of test carrier using D20 polishing pad.

The suitable polishing parameters (Table 5) of the PB20 polishing ball and the control P (Kp=0.1) were applied to polish the concave area of the freeform surface. The burnished surface roughness in the concave area improved from Ra $0.12~\mu m$ to $0.03~\mu m$ on average after polishing. Figure 21 presents the measured surface roughness of Ra $0.03~\mu m$. The improvement in surface roughness of the polished plane surface was about 75%. Table 9 summarize the surface roughness measurement results of the test carrier at different surface features.

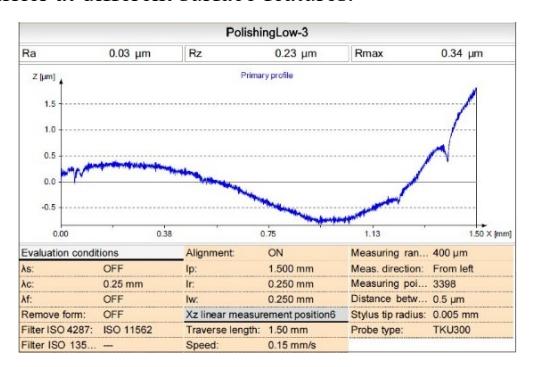


Fig. 21. Measured surface roughness of the polished concave area of test carrier using D20 polishing ball.

Table 9. Surface roughness measurement results of the test carrier at different surface features

Features	Surface roughness R _a (μm)			
1 catales	Fine milled	Burnished	Polished	
Plane surface	0.36	0.08	0.02	
Convex surface	0.89	0.18	0.04	
Concave surface	0.85	0.12	0.03	

Figure 22 presents the surface textures observed by a toolmaker's microscope in different areas of the test carrier. The surface roughness was found to be sequentially improved by fine milling, ball polishing, and robot-assisted polishing processes.

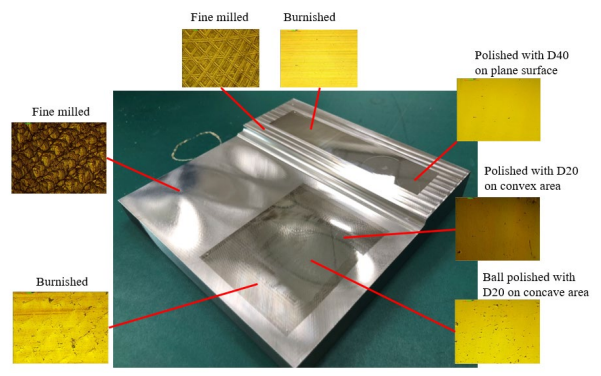


Fig. 22. Photo of the surface textures of the test carrier after fine milling, burnishing and polishing at different areas.

Volumetric Wear of the Lab-made Polishing Balls

The volumetric wears of the different polishing tools were calculated by their weight loss, as shown in Table 10. The wear rate ranges from 2.8 % (PD40) to 4.9 % (PD20), as shown in Table 10. The volumetric wear of the polishing pad PD20 is about 1.9 % greater

than the polishing ball PB20. The possible reason for that is the polishing force of PD20 (5.0 N) was five times than that of the polishing ball PB20 (1.0 N).

Table 10. Volumetric wear of different types of polishing tools

Features	Plane	Freeform surface	
Polishing tools	Polishing	Polishing	Polishing
	pad PD40	pad	ball
		PD20	PB20
Diameter (mm)	39.03	19.91	19.26
Weight before polishing (g)	7.86	2.60	3.16
Weight after polishing (g)	7.64	2.47	3.06
Volume before polishing	4797.68	1587.83	1928.85
(mm^3)			
Volume after polishing	4664.88	1509.37	1870.40
(mm ³)			
Wear volume (mm ³)	132.80	78.46	58.45
Wear rate (%)	2.8%	4.9%	3.03%

Discussion

Although the new polishing end effector clamping the lab-made polishing tools and the PID control system have been successfully applied to execute the robot assisted constant force polishing of a test carrier, there are still some issues to be discussed and investigated in the future.

- a. Regarding the calibration of the polishing force versus the depth of penetration for different polishing tools, the R-squared value (coefficient of determination) of 0.9985 was nearly perfect fit for the polishing ball PB20. For the polishing pads, the R-squared value decreased from 0.975 to 0.957 with an increase in the diameter from 20 mm to 40 mm. The possible reason might be the form error of the polishing pad increased as the diameter increased.
- b. Based on the analysis of variance (ANOVA), the dominant factor for the PB20 polishing ball was the abrasive size of 0.05 μm (Chen 2021). The dominant factors for the PD40 polishing pad were the abrasive size of 0.3 μm and the feeding rate of 0.1 mm/min in (Shih 2023). It was noticed that the polishing force was not one of the dominant factors for both polishing tools.
- c. Regarding the constant force polish control, a stable state could be achieved for three polishing tools, based on the experimental results in Figures 14, 16 and 17, respectively. However, it took about 50 to 150 seconds to reach the stable state. The Kp, Ki, and Kd gains of the PID control could be further improved, or a different control strategy might be investigated in the future.

CONCLUSION

A robot assisted constant force polishing system has been developed by integrating the new polish endeffector and the PID control system with a 6-axis industrial robot.

A new polishing end effector, mainly including a force sensor, overload prevention mechanism, spring,

and an electrical grinder, has been designed and fabricated, so a real-time constant force control was possible.

Three types of lab-made NBR-based polishing tools embedded with the abrasive of aluminum oxide were molded and tested. The suitable polishing parameters of the lab-made polishing tools for the STAVAX mold steel were determined by the Taguchi method. For a polish pad with a diameter of 40 mm PD40, the suitable parameters were the particle size of 0.3 μ m, spindle speed of 5,600 rev/min, feed rate of 0.1 mm/min, polishing force of 6 N. For the polishing ball with a diameter of 20 mm PB20, the recommended parameters were the particle size of 0.05 μ m, the spindle speed of 7,000 rev/min, the feed rate of 75mm/min, the polishing force of 1.0 N and the stepover of 0.01 mm.

The commonly used PID controller has been adopted to implement constant force polishing. The control gains Kp, Ki, and Kd of the PID controller were experimentally investigated for different polishing tools. Based on the test results, the PID gains for the PD40 polishing pad were Kp of 0.025, Ki of 0.015 and Kd of 0.0; The PI control (Kp=0.02 and Ki=0.005) was suitable for the PD20 polishing tool; The P control (Kp=0.01) was suitable for the PB20 polishing tool.

The optimal polishing parameters were applied to a test carrier with a plane surface and a freeform surface. The surface roughness of the plane area improved from Ra 0.36 μ mto Ra 0.02 μ m after sequential burnishing and polishing. For a burnished freeform surface area, the surface roughness was reduced from Ra 0.18 μ m to Ra 0.04 μ m on average, after the surface finishing using the polishing tool. Based on the experimental results, it can be confirmed that the surface roughness of the test carrier can be effectively improved by the developed polish end effector and the constant force PID control.

ACKNOWLEDGMENT

This research was sponsored by the Ministry of Science and Technology of the Republic of China (Taiwan) under grant NSTC 113-2221-E-011-084.

REFERENCES

- Almeida, R., Ebert, T., Börret, R. and Pohl, M., "Steel mould surface improvement by robot fluid jet polishing and robot pad polishing for polymer optic production," *EPJ Web of Conferences*, Vol. 215, 05003 (2019). https://doi.org/10.1051/epjconf/2019215050
- Chang, G., Pan, R., Xie, Y., Yang, J., Yang, Y., and Li, J., "Research on constant force polishing method of curved mold based on position adaptive impedance control," *The International Journal of Advanced*

- Manufacturing Technology, Vol. 122, pp. 697–709 (2022).
- Chen, B.Y., "Research on the constant force control of robot assisted polishing using lab-made polishing rubber tools", Master's thesis, Department of Mechanical Engineering, National Taiwan University of Science and Technology, (2021).
- Diaz-Rodriguez I., Han, S. and Bhattacharyya, S., Analytical Design of PID Controllers, Springer, (2019).
- Huang, S., Guo, Y., Huang, J., Yin, F. and Lu, J., "Research on Robotic Polishing Process of Marble with Complex Curved Surface Based on Sol–Gel Flexible Tools," *Applied Science*, Vol. 15, No. 1, 318, (2025). https://doi.org/10.3390/app15010318
- Huang, X., Wang Z. and Lin, Z., "Movement Modeling and Control for Robotic Bonnet Polishing," *Chinese Journal of Mechanical Engineering*, Vol. 35, No. 68, (2022). https://doi.org/10.1186/s10033-022-00751-y
- Ke, X., Yu, Y., Li, K., Wang, T., Zhong, B., Wang, Z., Kong, L., Guo, J., Huang, L., Idir, M. Liu, C. and Wang, C., "Review on robot-assisted polishing: Status and future trends," *Robotics and computer-Integrated Manufacturing*, Vol. 80, 102482 (2023). https://doi.org/10.1016/j.rcim.2022.102482
- Li, J., Guan, Y., Chen, H., Wang, B. and Zhang, T., "Robotic Polishing of Unknown-Model Workpieces with Constant Normal Contact Force Control," *IEEE/ASME Transactions on Mechatronics*, Vol 28, No. 2, (2023). https://doi.org/10.1109/TMECH.2022.32163
- Li, J., Huang, W., Xie, Y., Yang, J. and Zhao, M., "The parameters optimization of robotic polishing with force controlled for mold steel based on Taguchi method," *Journal of the Brazilian Society of Mechanical Sciences and Engineering*, Vol. 46, No. 313, (2024). https://doi.org/10.1007/s40430-024-04889-9
- Li, X., Zhao, H., Zhou, H., Cai, Y., Yin, Y. and Ding, H., "Robotic grinding and polishing of complex aeroengine blades based on new device design and variable impedance control," *Robotics and Computer-Integrated Manufacturing*, Vol. 92, 102875 (2025). https://doi.org/10.1016/j.rcim.2024.102875
- Lin, B., Jiang, X., Cao, Z. and Huang, T., "Development and theoretical analysis of novel center-inlet computer-controlled polishing process for high-efficiency polishing of optical surfaces," *Robotics and Computer-Integrated Manufacturing*, Vol. 59, pp.1–12. (2019).
- Liu, Y., Xi, F. and Faieghi, R.," Path Planning for Robotic Polishing of Sheet Metal Parts,"

- International Journal of Advanced Manufacturing Technology, Vol. 119, pp. 3303–3319 (2022).
- Phadke, M.S. *Quality Engineering Using Robust Design*; Pearson, India (2015).
- Shi, J., Dong J., Liu, C. and Yu T., "Control Strategy and Method for Variable Polishing Force Adapting to the 5-Axis Machining Trajectory," *Journal of Northeastern University (Natural Science)*, Vol. 41, No. 1, pp. 89-94 (2020).
- Shi, D., Zeng, X., Xuhui Wang, X. and Zhang, H., "Parameter Optimization and Surface Roughness Prediction for the Robotic Adaptive Hydraulic Polishing of NAK80 Mold Steel," *Processes*, Vol. 13, No. 4, 991 (2025). https://doi.org/10.3390/pr13040991
- Shih, W.Y., "Research on the surface polishing of the STAVAX mold steel with constant force control using lab-made polishing tools on a robot", Master's thesis, Department of Mechanical Engineering, National Taiwan University of Science and Technology, (2023).
- Shiou, F. and Hsu, C., "Surface finishing of hardened and tempered stainless tool steel using sequential ball grinding, ball burnishing and ball polishing processes on a machining centre," *Journal of Material Processing Technology*, Vol. 205, pp. 249–258 (2008).
- Shiou, F., Pan, J., Ding Z. and Lin, S., "Ultrasonic-Assisted Surface Finishing of STAVAX Mold Steel Using Lab-Made Polishing Balls on a 5-Axis CNC Machining Center," *Materials*, Vol. 16, No. 16, 5888 (2023). https://doi.org/10.3390/ma16175888
- STAVAX ESR Available online: https://www.assab.com/en/products/stavax-esr/ (2025).
- Wang, K., Dailami, F. and Jason Matthews, J., "Towards collaborative robotic polishing of mold and die sets," *Procedia Manufacturing*, Vol. 38, pp. 1499–1507 (2019).
- Wu, Z., Shen J., Peng Y. and Wu, X., "Review on ultra-precision bonnet polishing technology," *Int. J. Adv. Manuf. Technol.*, Vol. 121, pp. 2901–2921 (2022).
- Xiao, M., Ding, Y. and Yang, G., "A Model-Based Trajectory Planning Method for Robotic Polishing of Complex Surfaces," *IEEE Transactions on Automation Science and Engineering*, Vol. 19, No. 4 (2022). https://doi.org/10.1109/TASE.2021.3095061
- Xu, D. and Hu., T., "Modelling and vibration control of magnetorheological-based polishing tool for robotic polishing process," *Mechanical Systems and Signal Processing*, Vol. 195, 110290 (2023). https://doi.org/10.1016/j.ymssp.2023.110290